

Phase transformations and vibrational properties of coronene under pressure

Xiao-Miao Zhao, Jiang Zhang, Adam Berlie, Zhen-Xing Qin, Qiao-Wei Huang et al.

Citation: *J. Chem. Phys.* **139**, 144308 (2013); doi: 10.1063/1.4824384

View online: <http://dx.doi.org/10.1063/1.4824384>

View Table of Contents: <http://jcp.aip.org/resource/1/JCPSA6/v139/i14>

Published by the **AIP Publishing LLC**.

Additional information on *J. Chem. Phys.*

Journal Homepage: <http://jcp.aip.org/>

Journal Information: http://jcp.aip.org/about/about_the_journal

Top downloads: http://jcp.aip.org/features/most_downloaded

Information for Authors: <http://jcp.aip.org/authors>



www.goodfellowusa.com

Goodfellow

metals • ceramics • polymers
composites • compounds • glasses

Save 5% • Buy online
70,000 products • Fast shipping

Phase transformations and vibrational properties of coronene under pressure

Xiao-Miao Zhao,^{1,2} Jiang Zhang,¹ Adam Berlie,³ Zhen-Xing Qin,¹ Qiao-Wei Huang,^{1,2} Shan Jiang,⁴ Jian-Bo Zhang,¹ Ling-Yun Tang,¹ Jing Liu,⁵ Chao Zhang,^{6,7} Guo-Hua Zhong,⁸ Hai-Qing Lin,^{7,8} and Xiao-Jia Chen^{2,9,a)}

¹Department of Physics, South China University of Technology, Guangzhou 510640, China

²Center for High Pressure Science and Technology Advanced Research, Shanghai 201203, China

³Center for Energy Matter in Extreme Environments and Key Laboratory of Materials Physics, Institute of Solid State Physics, Chinese Academy of Sciences, Hefei 230031, China

⁴Analytical and Testing Center, South China University of Technology, Guangzhou 510640, China

⁵Institute of High Energy Physics, Chinese Academy of Sciences, Beijing 100190, China

⁶Department of Physics, Yantai University, Yantai 264005, China

⁷Beijing Computational Science Research Center, Beijing 100084, China

⁸Shenzhen Institutes of Advanced Technology, Chinese Academy of Sciences, Shenzhen 518055, China

⁹Geophysical Laboratory, Carnegie Institution of Washington, Washington, DC 20015, USA

(Received 11 July 2013; accepted 23 September 2013; published online 10 October 2013)

Both the vibrational and structural properties of coronene have been investigated upon compression up to 30.5 GPa at room temperature by a combination of Raman scattering and synchrotron x-ray diffraction measurements. The spectroscopic and crystallographic results demonstrate that two pressure-induced structural phase transitions take place at 1.5 GPa and 12.2 GPa where the high-pressure phases are identified as monoclinic and orthorhombic crystal structures with space groups of $P2_1/m$ and $Pmmm$, respectively. A kink in the slope of the cell parameters as a function of pressure is associated with the disappearance of several internal Raman modes, which suggests the existence of structural distortions or reorganizations at approximately 6.0 GPa. Above 17.1 GPa, almost no evidence of crystallinity can be observed, indicating a possible transformation of coronene into an amorphous phase. © 2013 AIP Publishing LLC. [<http://dx.doi.org/10.1063/1.4824384>]

I. INTRODUCTION

Polycyclic aromatic hydrocarbons (PAHs), that show extensive π -conjugation, have attracted much attention from chemists, physicists, and geoscientists because of their exceptional properties and extensive applications.^{1–3} Due to the relatively open-shell molecular units, their electronic properties can be modified by doping the pure phase with electron donors or acceptors, as is the case for the superconductivity recently discovered in potassium doped picene ($C_{22}H_{14}$). This discovery motivated the synthesis of a series of superconducting materials based on phenanthrene⁵ ($C_{14}H_{10}$), coronene⁶ ($C_{24}H_{12}$), and 1,2:8,9-dibenzopentacene⁷ ($C_{30}H_{18}$). Among these hydrocarbon based superconductors, the highest T_c observed was ~ 33 K in $K_{3,45}$ dibenzopentacene which surpasses the highest T_c (14.2 K at 8.2 GPa)⁸ achieved in charge-transfer organic superconductors. The pressure effect of such PAH superconductors is remarkable where the T_c of K_3 picene (18 K phase) increases linearly with pressure up to 1.2 GPa with $dT_c/dP = 12.5$ K GPa⁻¹,⁹ however, the 7 K phase exhibits a negative pressure dependence. Within the phenanthrene based superconductors, Wang *et al.*⁵ showed that T_c was enhanced by the application of pressure. In some cases, pressure may even be the decisive parameter in achieving superconductivity such as the highest T_c of 38 K ob-

served in Cs_3C_{60} ¹⁰ by the application of pressure. Thus, the application of pressure is of paramount importance to investigate superconductivity within organic based systems. Extensive investigations on PAHs have showed that pentacene, a straight-chain aromatic hydrocarbon, exhibited metallic character with a positive temperature coefficient of resistance at 27 GPa.¹¹ In addition, there is evidence that benzene enters a metallic phase at ~ 200 GPa as predicted by some theoretical work.¹² Therefore, the investigation of the parent compound of PAHs based superconductors under pressure is of great importance.

Coronene, is assembled in a concentric disk with seven benzene rings, which has been described previously.¹³ Pure coronene possesses monoclinic symmetry with two molecules per unit cell, the space group $P2_1/a$ and lattice parameters: $a = 16.094(9)$ Å, $b = 4.690(3)$ Å, $c = 10.049(8)$ Å, $\beta = 110.792(2)^\circ$. It has been established^{14,15} that the dramatic change of its polarized luminescence spectra indicates a temperature-induced phase transition in the temperature range from 140 K to 180 K and another structural phase transition at 50 K.¹⁶ In addition, a reversible phase transition between 2.0 and 3.2 GPa at room temperature was observed from Fourier-Transform Infrared spectroscopy experiments.¹⁷ In a prior study, electron-intramolecular-phonon coupling and its role in the occurrence of possible superconductivity in the monoanions of coronene have been studied.¹⁸ Furthermore, theoretical studies have attempted to account for the

^{a)}Electronic mail: xjchen@ciw.edu

nature of PAHs-based superconductor based on electron-phonon interaction.^{19–21} Knowledge of the physics properties and electron-phonon interaction of coronene at high pressures is helpful to understand the origin and mechanism of superconductivity in PAHs. In order to understand the intermolecular interaction and electron-phonon interaction of coronene, a thorough study focused on the molecular vibrational properties and structure evolution of coronene under pressure is highly needed.

In this paper, we have performed high-pressure Raman scattering using a near infrared (785 nm) excitation as well as synchrotron x-ray diffraction (XRD) measurements on coronene. The high-pressure Raman spectra up to 10.9 GPa at room temperature reveal two phase transitions at approximately 1.3 GPa and 3.7 GPa. Further structural investigation using XRD up to 30.5 GPa shows two structural phase transitions at 1.5 GPa and 12.2 GPa as well as a structural distortion or reorganization at approximately 6.0 GPa. At higher pressures, XRD results indicate a possible transformation into an amorphous phase.

II. EXPERIMENTAL DETAILS

Coronene (99% purity) was purchased from TCI Co. and used without further purification. High-pressure Raman experiments were conducted at room temperature using Diamond Anvil Cells (DACs) with beveled anvils and culets of 400 μm without a pressure-transmitting medium. A stainless steel gasket with a drilled hole of $\sim 130 \mu\text{m}$ in diameter was used as the sample chamber. To calibrate the pressure a small ruby chip was placed in the sample chamber with the samples whereby measuring the wavelength shift of the ruby R_1 fluorescence line²² gave an accurate measure of applied pressure. The LabRAM Aramis system with a spectrometer (with 1200 lines/mm grating) equipped with a di-monochromator and a charge coupled device detector was used for the measurement, achieving a spectral resolution of below 1 cm^{-1} . Raman spectra were obtained using a Raman microscope with a 785 nm stabilized diode-laser excitation.

Synchrotron XRD was carried out via the angle-dispersive experiments at the Beijing Synchrotron Radiation Facility (BSRF). Silicone oil was used as pressure transmitting medium to maintain quasi-hydrostatic pressure environment in the studied pressure range. The pressures were monitored by the ruby fluorescence shifts in the pressure range of 0.7–7.0 GPa. However, for pressure above 7.0 GPa, the signal of the ruby cannot be detected due to the fluorescence background. Therefore, we used a gold chip for pressure calibration at higher pressures. Comparison of both experiments shows the repeatability of the measurements, however, only the result of the first experiment is shown (pressures between 0.7 GPa and 7.0 GPa) as higher pressure shows strong contamination from the Au spectral intensity. The measurement was performed using a wavelength of 0.6199 \AA and the experimental parameters were calibrated with standard CeO_2 powder diffraction. The two-dimensional diffraction images were converted to 2θ versus intensity data plots using the FIT2D software.

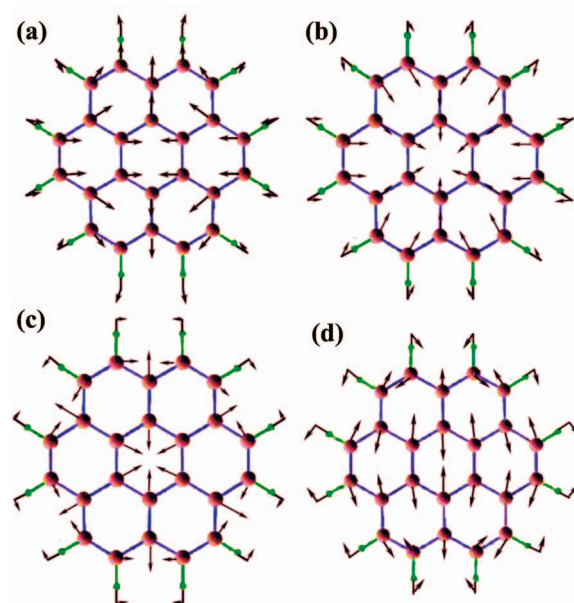


FIG. 1. Selected vibrational eigenmodes of coronene: (a) 354 cm^{-1} (E_{2g} -derived), (b) 481 cm^{-1} (A_{1g} -derived), (c) 1439 cm^{-1} (A_{1g} -derived), (d) 1666 cm^{-1} (E_{2g} -derived).

III. RESULTS AND DISCUSSION

A. High-pressure vibrational properties

Vibrational spectroscopy can make direct measurements on the state of bonding within the material at high pressures. According to the selection rules, there are 24 Raman-active modes in coronene: $6A_{1g}$, $6E_{1g}$, and $12E_{2g}$.²³ Four of these eigenvectors: 1666 cm^{-1} (E_{2g} -derived), 1439 cm^{-1} (A_{1g} -derived), 481 cm^{-1} (A_{1g} -derived), and 354 cm^{-1} (E_{2g} -derived) are shown in Fig. 1. Within our work, some low intensity modes, such as CH stretching located between 3000 and 3100 cm^{-1} could not be detected. The Raman modes observed in our study are listed in Table I where the initial spectrum taken at ambient pressure is in good agreement with those obtained in other theoretical and experimental studies.^{23–26} The similar vibrational properties have been investigated for phenanthrene²⁷ and picene.^{28,29}

Raman vibrational spectra of coronene collected at high pressures up to 10.9 GPa are shown in Fig. 2. For organic molecules the lattice and intramolecular vibrational modes are situated in different regions of frequency. Generally intramolecular modes, such as bond stretches and rotations, are located in the high-frequency region while the lattice modes, representing the translations and the rotations of rigid molecules, are seen in the low-frequency region. Within our data almost all the modes shift toward higher frequencies and some peaks are broadened with increasing pressure. The lattice modes exhibit more drastic changes than intramolecular modes, which are due to there being greater intermolecular distortions than intramolecular under applied pressure. On the basis of the splitting of doubly degenerate modes and the disappearance of well defined peaks as the pressure increased, it was confirmed that several pressure-induced phase transitions take place up to 10.9 GPa.

TABLE I. Assignment and frequencies (cm^{-1}) of observed Raman modes of coronene in comparison with references.

Raman modes	Assignment ^{a,b}	Reference		
		Calculation ^{a,b}	Experimental ^{c,d}	This work
L ₁	Lattice mode		77 ^d	73
L ₂	Lattice mode		90 ^d	96
ν_1	E_{2g} (C–C–C out-of-plane bending)	354 ^b	370	371
ν_2	E_{1g} (unassigned)	447	435 ^d	449
ν_3	A_{1g} (C–C–C out-of-plane bending)	481 ^b	484	488
ν_4	E_{2g} (C–H out-of-plane bending)	990		998
ν_5	E_{1g} (C–H in plane bending)	1029	1027	1028
ν_6	E_{2g} (Aromatic C–C stretching)	1211		1224
ν_7	A_{1g} (Aromatic C–C stretching)	1334	1351	1352
ν_8	A_{1g} (Aromatic C–C stretching)	1439 ^b	1369	1370
ν_9	A_{1g} (Aromatic C–C stretching)	1434		1438
ν_{10}	A_{1g} (Aromatic C–C stretching)	1447	1451	1452
ν_{11}	A_{1g} (Aromatic C–C stretching)	1603	1597	1599
ν_{12}	E_{2g} (Aromatic C–C stretching)	1617	1618	1618
ν_{13}	E_{2g} (Aromatic C–C stretching)	1666	1633 ^d	1632

^aFrom Ref. 24.^bFrom Ref. 23.^cFrom Ref. 25.^dFrom Ref. 26.

The lattice modes show an interesting behavior where the intensity of the L₂ mode is higher than L₁ at 0.1 GPa, however, at 0.4 GPa this reverses. This behavior points to the exchange of the symmetry of the two modes and may result from Fermi resonance.³⁰ At 1.3 GPa, the Raman modes L₁ and L₂ show a dramatic increase in frequency associated with the two lattice modes that appear at 115 cm^{-1} and 155 cm^{-1} and then disappear at 3.7 GPa. The peak at 371 cm^{-1} , associated with C–C–C out of plane bending, splits into two modes, losing its degeneracy which is coupled with the overlapping peaks initially located at 488 cm^{-1} becoming more separated with the increase of pressure. These features in the Raman spectra suggest substantial changes in the crystal and molecular structures at 1.3 GPa. With a further increase of pressure up to 3.7 GPa, a new peak emerges from lattice mode range, whilst the splitting of the mode at 449 cm^{-1} disappears. More interestingly, the overlapping peaks with the frequency of 488 cm^{-1} , corresponding to C–C–C out of plane bending, combine into a single peak above 3.7 GPa where the new peak may be a superposition of the two mode excitations. Again, the changes of vibrational modes indicate that another phase transition may occur in this region of pressure. Additionally, the intramolecular mode (originally at 371 cm^{-1}) shows a substantial broadening and loss of intensity above 3.3 GPa. Further increase of pressure up to 8.0 GPa shows a decrease in intensity associated with the lattice modes to the point where they are lost in the increasing fluorescence background.

For the higher frequencies significant changes can also be observed as pressure increases. The overlapping peaks (initially located at approximately 1599 cm^{-1}) merge into a single peak at 1.3 GPa. The modes with frequencies 1028 cm^{-1} , 1224 cm^{-1} , and 1352 cm^{-1} are weakened and broadened by rotations and molecular interaction (vibrational relaxation)

with the increasing pressure. The peak at 998 cm^{-1} corresponding to C–H out-of-plane bending disappears at approximately 3.3 GPa, while the band located at 1028 cm^{-1} , assigned to the C–H in plane bending, is sustained up to 6.8 GPa. This phenomenon seems to suggest that the molecular structure of coronene³¹ is compressed into 2D planes by high pressure, thus the C–H out-of-plane bending is unfavorable due to increasing electrostatic repulsion of the atoms by the molecules above and below each coronene molecule. The modes at 998, 1224, and 1438 cm^{-1} disappear as the pressure up to 3.7 GPa. Furthermore, two modes merge into a peak at frequency of 1618 and 1632 cm^{-1} , which again provides further evidence for a phase transition taking place. With increasing pressure to 8.0 GPa, most of Raman peaks disappear except that the modes of 1352 cm^{-1} and 1370 cm^{-1} combine into a broad peak, which vanishes at the pressure of 10.9 GPa.

In order to precisely determine the pressure at which phase transitions take place the pressure dependencies of Raman modes have been plotted out in Fig. 3. It is clear that there are obvious discontinuities in the data at 1.3 GPa and 3.7 GPa confirming our conclusion of pressure induced phase transitions. There are two main pressure effects on the crystal vibrations: large shifts of the modes in the lattice modes region and slight modification of the intramolecular modes in the high-frequency region. Upon compression to 1.3 GPa, the lattice modes undergo a dramatic change where the van der Waals forces between molecules are altered due to the decrease of intermolecular space. Furthermore, two modes at 371 and 449 cm^{-1} lose their degeneracy and split into two separate modes at 1.3 GPa, also providing evidence of phase transition at 1.3 GPa. It is worth noting that the aromatic C–C stretching vibrational mode of ν_4 shows a negative frequency shift with increasing pressure to 0.9 GPa. This

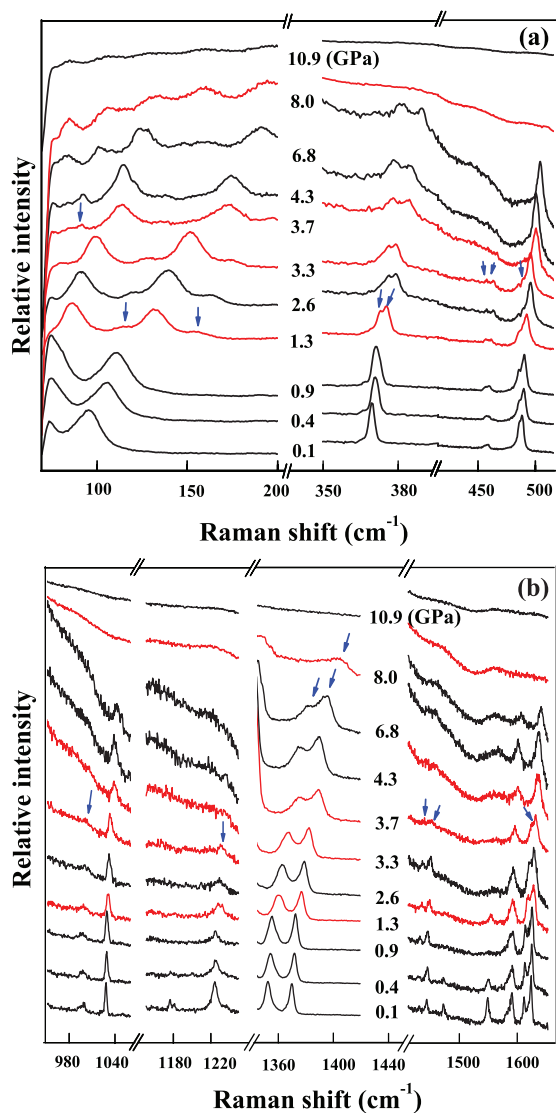


FIG. 2. Raman spectra up to 10.9 GPa. (a) Representative Raman spectra of coronene in the low frequency range of 60–520 cm^{-1} , (b) Selected Raman spectra of coronene in the high frequency range of 950–1700 cm^{-1} . The arrows indicate the changes of Raman modes.

slight softening against pressure may arise from the rotation of molecules. When compressed to 3.7 GPa the sample undergoes a second phase transition where the lattice mode at 115 cm^{-1} and the internal modes of ν_2 , ν_4 , ν_9 , and ν_{10} disappear. A further increase of pressure to 8.0 GPa, the Raman modes are significantly obscured and vanish at 10.9 GPa. The disappearance of Raman modes is possibly due to the generation of fluorescence (Rayleigh scattering), analogous to aceto-phenone azine,³² and may also be due to the transformation of coronene into a disordered material similar to the amorphous hydrogenated carbon structure obtained in the pressure-induced reactivity of benzene.^{33–35} The occurrence of fluorescence may also result from the shortened distance between molecules at high pressures where one may observe orbital overlap between two adjacent π -conjugated molecules (creating a new molecular orbital across two molecules),³² or from excited structural defects similar to pyrene.³⁶

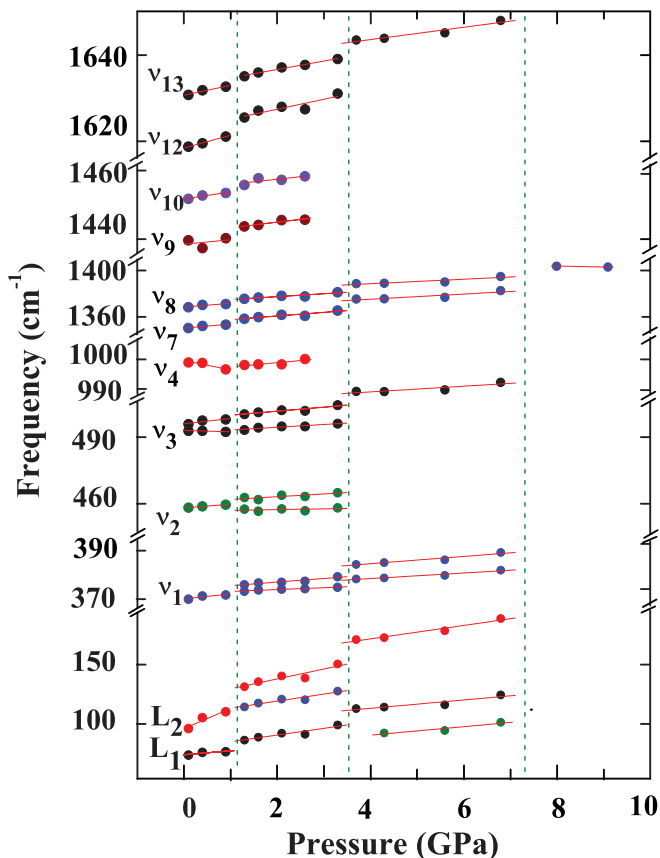


FIG. 3. Pressure dependence of vibrational frequencies observed in coronene at room temperature. The vertical dotted lines located at near 1.3 GPa and 3.7 GPa indicate possible phase boundaries.

B. Analysis of structural evolution with pressure

In order to further explore the pressure dependence of coronene, high-pressure XRD measurements were performed up to 30.5 GPa. Figure 4 shows some representative XRD patterns collected under various pressures at room temperature. The ambient condition diffraction data (phase I) can be fit using the space group $P2_1/a$ and the fitted results are shown in Fig. 5(a). The lattice parameters calculated from the fitted results are $a = 16.0929(6)$ Å, $b = 4.6835(7)$ Å, $c = 10.0600(6)$ Å, and $\beta = 111^\circ$, which are in good agreement with previously reported data.¹³ When looking at the evolution of the diffraction patterns as a function of applied pressure (Fig. 4) the peak positions shift to higher angles (smaller d -spacing) as the crystal structure is compressed. Upon compression to 0.7 GPa, the XRD pattern exhibits a dramatic changes in the number, intensity, and sharpness of peaks. It appears that the phase change is completed at 1.5 GPa, consistent with the Raman spectroscopy data. Compression up to 12.2 GPa shows a decrease and broadening in peak intensities, accompanied with the disappearance of several diffraction peaks (see arrows in Fig. 4). At pressures above 17.1 GPa, almost no signal of crystallinity can be detected, except for the only diffraction peak at approximately $2\theta = 4^\circ$ ($d = 8.877$ Å), corresponding to (001) diffraction peak at ambient condition with the space group $P2_1/a$. The characteristic length is related to the distance of intermolecular of coronene.

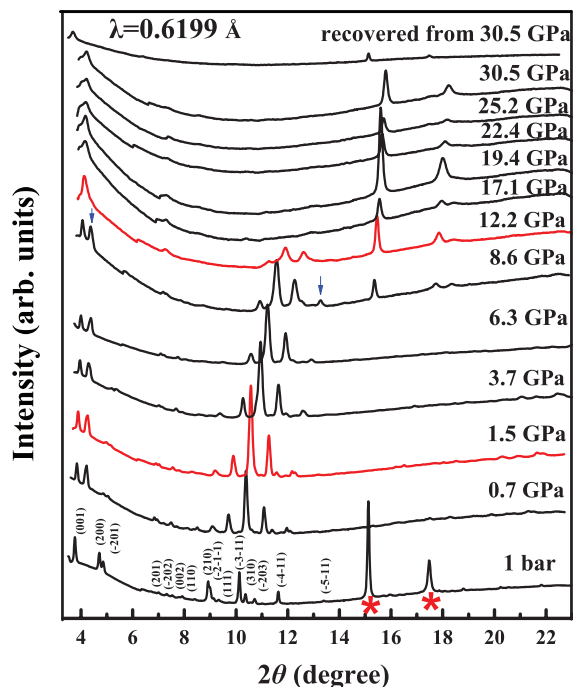


FIG. 4. Pressure evolution of the XRD ($\lambda = 0.6199 \text{ \AA}$) patterns of coronene and the XRD pattern of sample decompression from 30.5 GPa (top of figure). The pressures were determined by the wavelength shift of the ruby fluorescence at pressures between 0.7 GPa and 7.0 GPa. The other pressures were then calibrated by a gold chip where the diffraction peaks are marked with asterisks.

To further investigate the structural evolution under pressure, full refinements of diffraction patterns up to 14.4 GPa using the Le Bail method with GSAS software were carried out.³⁷ Since there is little information of the crystal structure available for coronene at high pressures, the possible crystal structures of unknown phases were analyzed with the programs DICVOL 06^{38,39} and PEAKFIT V4.

For phase II, the XRD pattern at 5.7 GPa was indexed as a low symmetry system with either a monoclinic or orthorhombic unit cell. According to the Raman spectroscopy results, both the splitting of several bands and the appearance of new peaks provide evidences for lower symmetry within phase II. In addition, when we attempt to fit the pattern with a body centered orthorhombic structure, such as the space groups of $I222$, $I2_12_12_1$, $Immm$, $Immm$, $Iba2$, $Ibam$, $Ibca$, and $Imma$, as previously suggested,¹⁴ the fitted results are poor. Therefore, since it was not possible to fit the data with a body centered orthorhombic structure, this can be safely ruled out. A better fit to the data was provided when using a monoclinic space group, such as $P2_1/m$, which showed a good fit to the data, as shown in Fig. 5(b). The lattice parameters were calculated to be $a = 16.4358(9) \text{ \AA}$, $b = 4.5584(7) \text{ \AA}$, $c = 8.9553(8) \text{ \AA}$, and $\beta = 100^\circ$. Although the XRD diffraction pattern at 0.7 GPa is similar to that at 1.5 GPa data, several characteristic peaks of $P2_1/a$ were also observed, which indicate a transient phase at 0.7 GPa.

In Fig. 4, there is a change at 12.2 GPa where the third phase (phase III) was indexed as either monoclinic or orthorhombic. Previously reported data¹⁴ show that the x-ray diffraction pattern at 1.8 GPa is similar to an orthorhombic

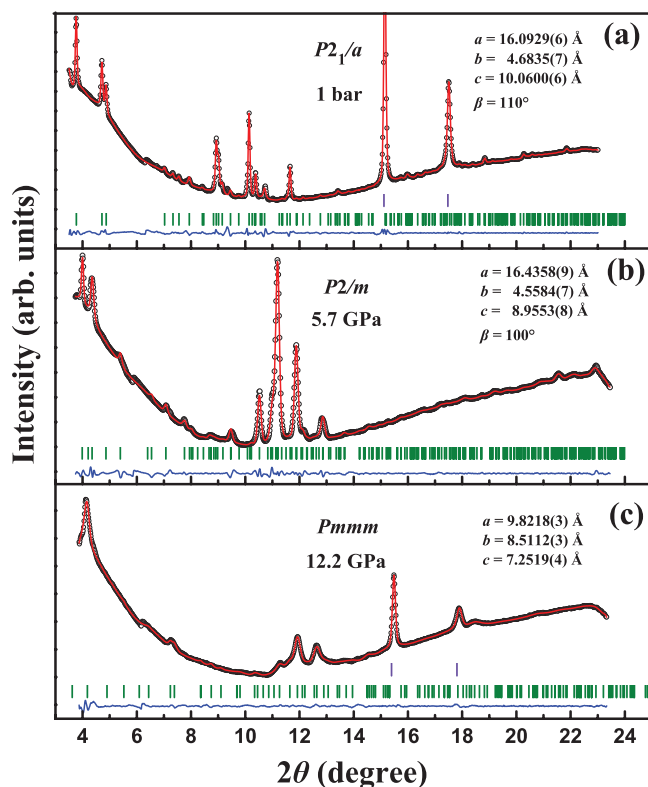


FIG. 5. XRD patterns of coronene at various pressures where the refined lattice parameters for the corresponding space groups are also included. The open circles represent the measured intensities and the red lines the results of profile refinements by the best LeBail fit with each space group. The positions of the Bragg reflections are marked by vertical lines and the difference profiles are shown at the bottoms (blue lines). The R values are (a) $R_p = 0.3\%$, $R_{wp} = 0.5\%$ for the fitting at 1 bar, (b) $R_p = 0.3\%$, $R_{wp} = 0.4\%$ at 5.7 GPa, and (c) $R_p = 0.2\%$, $R_{wp} = 0.3\%$ at 12.2 GPa.

system, however, one peak could not be assigned. Taking the above Raman spectroscopy results into consideration, the number of Raman active bands decrease with increasing pressure above 3.7 GPa, indicating the material possesses higher structural symmetry at higher pressures. The monoclinic system can be ruled out due to unreasonable figures of merit (M,F) and/or illogical volume of the cell. Thus, it can be reasonably assumed that the structure changes completely into an orthorhombic structure under high pressure. We choose an orthorhombic structure with the space group $Pmmm$ to fit the patterns of XRD above 12.2 GPa based on the indexed results. The difference between the observed and the calculated XRD intensity distribution is reasonable where Fig. 5(c) shows the fitted results for phase III (12.2 GPa) with the space group $Pmmm$ with unit cell parameters of $a = 9.8218(3) \text{ \AA}$, $b = 8.5112(3) \text{ \AA}$, and $c = 7.2519(2) \text{ \AA}$.

The pressure dependence of the lattice parameters a , b , and c up to 14.4 GPa studied at room temperature is plotted in Fig. 6. From discontinuities in the data one can assign phase transitions as a function of pressure. The first occurs at approximately 1.5 GPa, consistent with the observed 1.3 GPa phase transition in the Raman spectroscopy data (see Fig. 3). For phase II at the lower pressures below 6.0 GPa the lattice of coronene is much more compressible in the longer a

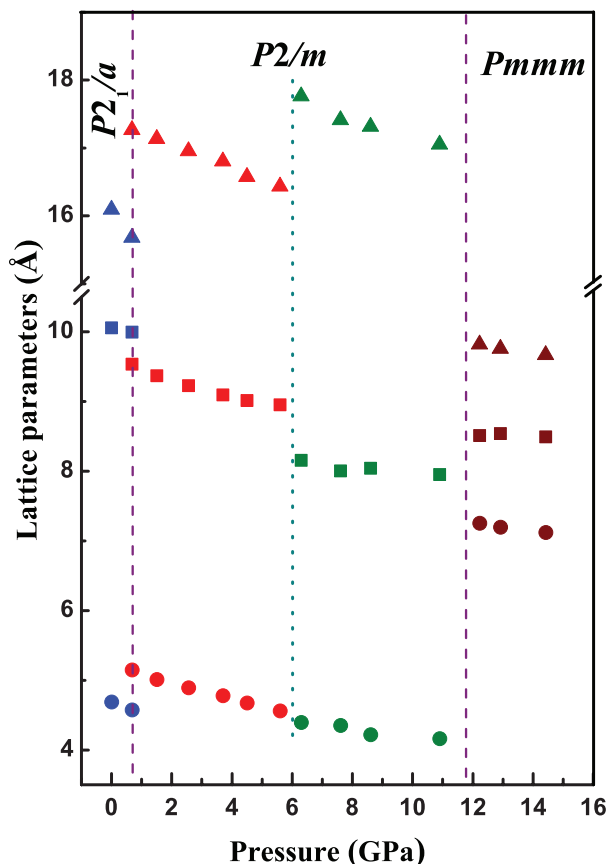


FIG. 6. Cell parameters of coronene versus pressure up to 14.2 GPa. The vertical dashed lines indicate the phase boundaries and the vertical dotted lines denote the structural distortions point. The squares correspond to changes in the a axis, the solid circles represent the b axis, and triangles denote the c axis. The space groups for the high-pressure phases were determined to be $P2_1/a$ for phase I, $P2/m$ for phase II, and $Pmmm$ for phase III.

axis than the shorter c axis while the angle β keeps constant at 99° . It is worth noting that in the high pressure region of phase II the lattice parameters of a and b show a discontinuity at 6.0 GPa, while the angle β exhibits a step decrease to 95° , however, there is no variation in volume. A kink in the pressure slope of lattice parameters results from the changes of the crystalline orientation or structural reorganizations of the molecules themselves. The structural distortions or reorganizations at approximately 6.0 GPa is consistent with the phase transition at 3.7 GPa observed in the Raman spectra. Raman spectroscopy can probe local molecular distortions, however, using XRD, one is sensitive to only bulk changes. The slightly different critical pressures between Raman and XRD can be explained in terms of nonhydrostatic pressure environment in Raman measurement. For phase III, all the three cell parameters are almost pressure-independent, which suggests the material has become a much more tightly crystal packed structure.

Figure 7 plots the unit cell volume V as a function of pressure at room temperature, together with the least-squares fit to the semi-empirical second-order Murnaghan equation of states (EOS)^{40,41} defined as $P = (K_0/K'_0)[(V_0/V)^{K'_0} - 1]$ where K_0 is the isothermal bulk modulus, K'_0 is the pressure derivative ($=dK_0/dP$), and V_0 is the volume of the unit cell at

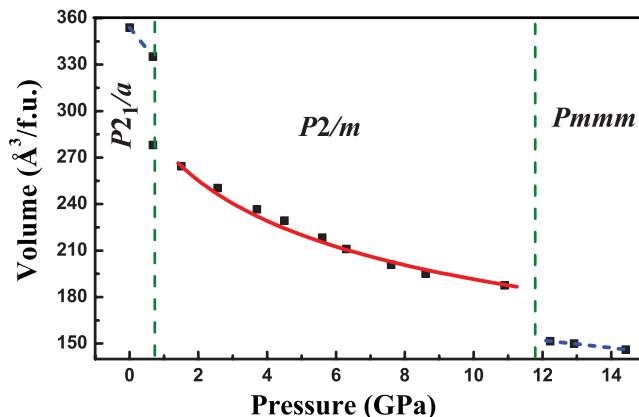


FIG. 7. Volume per formula unit change of coronene with pressure. The solid lines show the least-squares fit to the second-order Murnaghan equation of states and the vertical dashed lines indicate the phase boundaries.

zero pressure. The fit to the data within the phase II region results in values of $K_0 = 6.8(5)$ GPa and $K'_0 = 4$ where the value of bulk modulus is in agreement with anthracene,^{42,43} which is in the range of 6.5–7.5 GPa. Within phase II, van der Waals interactions play a dominant role, which leads to the small value of the bulk modulus. A slow change of unit cell volume is probably associated with the intramolecular interaction where for phase III a dramatic change indicates that the coronene molecules are forced to change into a more compact, higher symmetry, configuration at high pressure. The figure also illustrates the two structural changes at 1.5 and 12.2 GPa.

It is worth noting that above 17.1 GPa almost no signal of crystallinity can be detected except for one peak which exists up to 30.5 GPa. Interestingly, the peak is the only reversible diffraction peak when decompressed from 30.5 GPa, showing the structure has undergone an irreversible change on compression where coronene may transform into amorphous clustered regions under pressure. The XRD data exhibit that all the lattice parameters become almost pressure independent above 12.2 GPa, indicating that the intermolecular distance is small enough to form a highly incompressible phase, analogous to high-pressure behavior of C_{60} *m-xylene.⁴⁴ Furthermore, the XRD pattern up to 30.5 GPa is also similar to those observed in compressed C_{60} *m-xylene, where unsaturated carbon atoms are converted into saturated carbon under applied pressure, giving a further evidence for transformation of coronene into an amorphous phase.

IV. CONCLUSIONS

We have investigated the structural and vibrational properties of coronene at high pressures up to 30.5 GPa by a combination of Raman scattering and synchrotron x-ray diffraction measurements. High pressure Raman spectra of coronene revealed two phase transitions at 1.3 GPa and 3.7 GPa where the different phases are due to changes in both inter- and intramolecular distances. Synchrotron XRD was used to investigate the pressure-dependence of the structure up to 30.5 GPa at room temperature. The results indicate two structural transitions at 1.5 GPa and 12.2 GPa where the space groups for

the high-pressure phases were determined to be $P2_1/a$ for phase I (ambient), $P2/m$ for phase II ($1.5 \leq P \leq 12.2$ GPa), and $Pmmm$ for phase III ($P \geq 12.2$ GPa). The change of lattice parameters in phase II suggests there is structural distortion or reorganization at approximately 6.0 GPa, coinciding with the results observed from Raman spectra. At higher pressure, coronene transforms into an amorphous phase where the original crystal structure could not be recovered on decompression. These subtle changes in crystal structure may facilitate research into the mechanism of superconductivity at high pressures within organic based materials.

ACKNOWLEDGMENTS

This work was supported as part of EFree, an Energy Frontier Research Center funded by the U.S. Department of Energy (DOE), Office of Science under Grant No. DE-SC0001057. The work done in China was supported by the Cultivation Fund of the Key Scientific and Technical Innovation Project Ministry of Education of China (Grant No. 708070), the Shenzhen Basic Research (Grant No. JC201105190880A), the National Natural Science Foundation of China (Grant No. 11274335), and Guangdong Natural Science Foundation (Grant No. S2012040007929).

- ¹E. A. Silinsh and V. Capek, *Organic Molecular Crystals: Interaction, Localization, and Transport Phenomena* (Springer-Verlag, Berlin, Heidelberg, and New York, 1994).
- ²R. Farchioni and G. Grosso, *Organic Electronic Materials: Conjugated Polymers and Low Molecular Weight Organic Solids* (Springer, Berlin, 2001).
- ³L. J. Allamandola, S. A. Sandford, and B. Wopenka, *Science* **237**(4810), 56 (1987).
- ⁴R. Mitsuhashi, Y. Suzuki, Y. Yamanari, H. Mitamura, T. Kambe, N. Ikeda, H. Okamoto, A. Fujiwara, M. Yamaji, N. Kawasaki, Y. Maniwa, and Y. Kubozono, *Nature Commun.* **464**, 76 (2010).
- ⁵X. F. Wang, R. H. Liu, Z. Gui, Y. L. Xie, Y. J. Yan, J. J. Ying, X. G. Luo, and X. H. Chen, *Nature Commun.* **2**, 507 (2011).
- ⁶Y. Kubozono, H. Mitamura, X. Lee, X. He, Y. Yamanari, Y. Takahashi, Y. Suzuki, Y. Kajii, R. Eguchi, K. Akaike, T. Kambe, H. Okamoto, A. Fujiwara, T. Kato, T. Kosugi, and H. Aoki, *Phys. Chem. Chem. Phys.* **13**, 16476 (2011).
- ⁷M. Q. Xue, T. B. Cao, D. M. Wang, Y. Wu, H. X. Yang, X. L. Dong, J. B. He, F. W. Li, and G. F. Chen, *Sci. Rep.* **2**, 389 (2012).
- ⁸H. Taniguchi, M. Miyashita, K. Miyashita, K. Satoh, N. Mōri, H. Okamoto, K. Miyagawa, K. Kanoda, M. Hedo, and Y. Uwatoko, *J. Phys. Soc. Jpn.* **72**, 468 (2003).
- ⁹T. Kambe, X. He, Y. Takahashi, Y. Yamanari, K. Teranishi, H. Mitamura, S. Shibusaki, K. Tomita, R. Eguchi, H. Goto, Y. Takabayashi, T. Kato, A. Fujiwara, T. Kariyado, H. Aoki, and Y. Kubozono, *Phys. Rev. B* **86**, 214507 (2012).
- ¹⁰A. Y. Ganin, Y. Takabayashi, Y. Z. Khimyak, S. Margadonna, A. Tamal, M. J. Rosseinsky, and K. Prassides, *Nature Mater.* **7**, 367 (2008).
- ¹¹R. B. Aust, W. H. Bentley, and H. G. Drickamer, *J. Chem. Phys.* **41**, 1856 (1964).

- ¹²X. D. Wen, R. Hoffmann, and N. W. Ashcroft, *J. Am. Chem. Soc.* **133**, 9023 (2011).
- ¹³J. K. Fawcett and J. Trotter, *Proc. R. Soc., London, Ser. A* **289**, 366 (1966).
- ¹⁴T. Yamamoto, S. Nakatani, T. Nakamura, K. Mizuno, A. H. Matsui, Y. Akahama, and H. Kawamura, *Chem. Phys.* **184**, 247 (1994).
- ¹⁵R. Totoki, T. Aoki-Matsumoto, and K. Mizuno, *J. Lumin.* **112**, 308 (2005).
- ¹⁶S. Nakatani, T. Nakamura, K. Mizuno, and A. Matsui, *J. Lumin.* **58**, 343 (1994).
- ¹⁷E. Jennings, W. Montgomery, and Ph. Lerch, *J. Phys. Chem.* **114**, 15753 (2010).
- ¹⁸T. Kato, K. Yoshizawa, and K. Hirao, *J. Chem. Phys.* **116**, 3420 (2002).
- ¹⁹M. Casula, M. Calandra, G. Profeta, and F. Mauri, *Phys. Rev. Lett.* **107**, 137006 (2011).
- ²⁰A. Subedi and L. Boeri, *Phys. Rev. B* **84**, 020508(R) (2011).
- ²¹T. Kato, T. Kambe, and Y. Kubozono, *Phys. Rev. Lett.* **107**, 077001 (2011).
- ²²H. K. Mao, P. M. Bell, J. W. Shaner, and D. J. Stembey, *J. Appl. Phys.* **49**, 3276 (1978).
- ²³C. Thomsen, M. Machón, and S. Bahrs, *Solid State Commun.* **150**, 628 (2010).
- ²⁴U. Fleischer and P. Pulay, *J. Raman Spectrosc.* **29**, 473 (1998).
- ²⁵L. Colangeli, V. Mennella, G. A. Baratta, E. Bussoletti, and G. Strazzulla, *Astrophys. J.* **396**, 369 (1992).
- ²⁶K. Ohno, T. Kajwara, and H. Inokuchi, *Bull. Chem. Soc. Jpn.* **45**, 996 (1972).
- ²⁷Q. W. Huang, J. Zhang, A. Berlie, Z. X. Qin, X. M. Zhao, J. B. Zhang, L. Y. Tang, J. Liu, C. Zhang, G. H. Zhong, H. Q. Lin, and X. J. Chen, *J. Chem. Phys.* **139**, 104302 (2013).
- ²⁸S. Fanetti, M. Citroni, L. Malavasi, G. A. Artioli, P. Postorino, and R. Bini, *J. Phys. Chem. C* **117**, 5343 (2013).
- ²⁹F. Capitani, M. Höppner, B. Joseph, L. Malavasi, G. A. Artioli, L. Baldassarre, A. Perucchi, M. Piccinini, S. Lupi, P. Boeri, and P. Postorino, "A combined experimental and computational study of the pressure dependence of the vibrational spectrum of solid picene $C_{22}H_{14}$," e-print [arXiv:1306.1030](https://arxiv.org/abs/1306.1030) [cond-mat.supr-con] (unpublished).
- ³⁰Y. Lin, W. L. Mao, V. Drozd, J. H. Chen, and L. L. Daemen, *J. Chem. Phys.* **129**, 234509 (2008).
- ³¹P. D. Todorov, L. W. Jenneskens, and J. H. van Lenthe, *J. Chem. Phys.* **132**, 034504 (2010).
- ³²X. D. Tang, Z. J. Ding, and Z. M. Zhang, *Solid State Commun.* **149**, 301 (2009).
- ³³L. Ciabini, M. Santoro, R. Bini, and V. Schettino, *J. Chem. Phys.* **116**, 2928 (2002).
- ³⁴L. Ciabini, M. Santoro, R. Bini, and V. Schettino, *Phys. Rev. Lett.* **88**, 085505 (2002).
- ³⁵L. Ciabini, M. Santoro, F. A. Gorelli, R. Bini, V. Schettino, and S. Raugei, *Nature Mater.* **6**, 39 (2006).
- ³⁶B. Sun, Z. A. Dreger, and Y. M. Gupta, *J. Phys. Chem.* **112**, 10546 (2008).
- ³⁷A. C. Larson and R. B. Von-Dreele, GSAS-General Structure Analysis System. Report LAUR 86-748, Los Alamos National Laboratory, USA, 1994.
- ³⁸A. Boulitif and D. Louer, *J. Appl. Crystallogr.* **37**, 724 (2004).
- ³⁹D. Louer and A. Boulitif, *Z. Kristallogr. Suppl.* **26**, 191 (2007).
- ⁴⁰F. D. Murnaghan, *Proc. Natl. Acad. Sci. U.S.A.* **30**, 244 (1944).
- ⁴¹J. R. Macdonald and D. R. Powell, *J. Res. Natl. Bur. Stand., Sect. A* **75A**, 441 (1971).
- ⁴²S. N. Vaidya and G. C. Kennedy, *J. Chem. Phys.* **55**, 987 (1971).
- ⁴³M. Oehzelt, G. Heimel, R. Resel, P. Puschnig, and K. Hummer, *J. Chem. Phys.* **119**, 1078 (2003).
- ⁴⁴L. Wang, B. B. Liu, H. Li, W. G. Yang, Y. Ding, S. V. Sinogeikin, Y. Meng, Z. X. Liu, X. C. Zeng, and W. L. Mao, *Science* **337**, 825 (2012).